JOURNAL OF MATERIALS SCIENCE 30 (1995) 3995–4002

Processing of bulk $YBa_2Cu_3O_{7-\delta}$ ceramics prior to peritectic solidification

WAI LO, D. A. CARDWELL, S.-L. DUNG, R. G. BARTER
IRC in Superconductivity, University of Cambridge, Madingley Road, Cambridge CB3 OHE, UK

The influence of the physical and chemical properties of precursor green bodies on the properties of fully melt-processed $YBa_2Cu_3O_{7-\delta}$ ceramic (YBCO) have been investigated. Cold isostatic pressing has been found to allow better control of the size and distribution of Y_2BaCuO_5 phase inclusions in the melt-processed ceramic than a combination of die pressing and sintering. A study of the loss of liquid from YBCO during partial melting has revealed that the total percentage weight loss is sensitive to both the heating rate and proportion of excess 211 phase and is maximum at a temperature corresponding to the peak of the differential thermal analysis partial melting endotherm. Densification and expansion processes in the sample, which compete during melting, have been investigated in detail. The temperature where the expansion rate is maximum has been found to coincide with the maximum rate of oxygen desorption by the sample. The expansion process terminates on completion of partial melting whereas the densification process, which is dominated by the volume proportion of liquid, continues but at a reduced rate. The use of dense green bodies and an optimum heat-treatment process has been found to be essential for the fabrication of large-grain melt-processed YBCO if a fine distribution of 211 phase inclusions and the homogeneity and shape of the sample are to be retained.

1. Introduction

A variety of melt-processing techniques have been used to fabricate large-grain $YBa_2Cu_3O_{7-\delta}$ ceramics (YBCO) which exhibit critical current densities of up to 50 000 A cm^{-2} at 77 K and 1 T [1–4]. This represents a significant improvement over the critical current densities of sintered YBCO, which are around 1 000 A cm^{-2} [5], and highlights the potential of melt-processed materials for a number of high-field engineering applications such as magnetic bearings, fault current limiters and current leads [6–8]. Significantly, the best melt-processed $YBa_2Cu_3O_{7-\delta}$ (the so-called 123 phase) typically contains a fine, unconnected dispersion of Y_2BaCuO_5 phase material (the so-called 211 phase) embedded in the 123 matrix [1, 2, 9–11] which is not present in sintered material. The presence of this second phase in melt-processed samples is considered to enhance their ability to pin magnetic flux and hence account for the observed increase in critical current density [12]. Control of the formation of the 211 phase during melt processing is considered essential, therefore, if material with the required electrical and magnetic properties is to be fabricated.

All melt-processing techniques used to fabricate large-grain YBCO ceramics exploit a peritectic reaction at 1015 °C from which the 123 phase is formed from the 211 phase and a $3BaCuO_2 + 2CuO$-based liquid phase (L), i.e.

$$\underset{(211)}{Y_2BaCuO_5} + \underset{(L)}{3BaCuO_2 + 2CuO} \rightarrow \underset{(123)}{2YBa_2Cu_3O_{6.5}} \quad (1)$$

The 211 phase and the liquid in this reaction can be produced by rapidly heating a presintered green body of the desired composition to a temperature well above the peritectic temperature, T_p. Formation of the required 123 phase is then achieved by cooling the partially molten YBCO material slowly through T_p. It is desirable to add up to 30 mol % of the 211 phase to the 123 phase prior to melt processing, both to generate more flux pinning sites and to prevent loss of liquid during melting. Semisolid solidification processes [13], such as that described by Equation 1, place certain requirements on the precursor YBCO green body if melt processing is to be performed effectively. Firstly the 211 phase particles in Y_2BaCuO_5-enriched $YBa_2Cu_3O_{7-\delta}$ should remain fine in the green body state if they are to form a fine dispersion in the fully melt-processed material. Secondly, the material must be able to retain the liquid phase resulting from the peritectic reaction within its bulk at temperatures significantly above T_p to enable formation of the 123 phase on cooling. This depends on the homogeneity and density of the precursor green body and on the size distribution of the 211 phase particles it contains. Finally, the green body should be free from compositional and surface contaminants which form heterogeneous grain nucleation sites and hence limit the grain size that can be achieved during the growth process.

The purpose of this study was to investigate the influence of the physical and chemical properties of precursor green bodies, prepared using a variety of

0022–2461

TABLE I A summary of the preparation conditions of the bulk specimens prior to melt processing

Specimen	Preparation technique	Remark
1	Die pressing	Pressure = 50 MPa
2	CIP of specimen 1	Pressure = 500 MPa
3	Sintering of specimen 1	At 930 °C for 8 h
4	Sintering of specimen 2	At 930 °C for 8 h

techniques, on the properties of the fully melt-processed ceramic. These will then be used to optimize the heat-treatment process of the materials prior to peritectic solidification.

2. Experimental procedure

2.1. Green body processing

A spray drying and calcination technique was used to prepare the YBCO precursor powder, as reported in detail elsewhere [14]. A cation stoichiometry of Y:Ba:Cu = 1.6:2.3:3.3 was employed initially, corresponding to a 30 mol % enrichment of the 123 phase by 211. The average size of the particles in the precursor powder was less than 3 μm diameter, with a significant fraction smaller than 0.2 μm. The precursor powders were used initially to investigate the effect of pressing conditions on the properties of the green body, as summarized in Table I. This involved pressing powder samples both uniaxially in a die and isostatically. A 13 mm diameter die was used in the former with a pressure of 50 MPa. Cold isostatic pressing (CIP) was performed under a pressure of 500 MPa (i.e. an order of magnitude higher than for the die-pressing case). These samples were sintered at 930 °C for 8 h in a box furnace to produce uniform precursor green bodies from which accurate density calculations could be made by simply weighing the specimens and measuring their dimensions with a micrometer.

2.2. Weight loss during melting

Loss of weight during melting has been investigated against key variables, such as oxygen desorption and high-temperature liquid loss, for three groups of specimens, as summarized in Table II. The first group (specimens 5–9) consisted of coarse particles of pure 123 phase material (typically in the region of 10–20 μm diameter), processed with varying heating rates. The fraction of 211 phase enrichment was varied in the second group of specimens (10–14) which were also characterized by a coarse particle size but were processed with a constant heating rate. The final group (specimens 15–21) consisted of fine particles with a fixed 211-phase enrichment and a constant heating rate. The degree of melting in these specimens was controlled by rapid cooling from different temperatures, as indicated in Table II. A constant specimen diameter and thickness of 3 and 1 mm, respectively, was employed in each case to eliminate systematic processing errors as far as possible. Heat treatment was performed and monitored by a Stanton Redcroft STA 1500 Thermal Analyser, which enabled simultaneous differential thermal and thermogravimetric analyses to be performed. Al_2O_3 crucibles were used for all the heat treatments and a high cooling rate (about 600 °C h^{-1}) was employed throughout in an attempt to minimize any sample–crucible interaction. Liquid loss during melting was estimated by weighing the specimens before and after the heat treatment.

2.3. Densification during melting

The bulk densities of specimens 15–21 (characterized by different quench temperatures and hence different degrees of melting) could be calculated accurately because they exhibited a uniform geometry after heat treatment. In order to study the densification and expansion processes during melting in the bulk specimens in more detail, however, YBCO pellets prepared from spray-dried precursor powder were melted at

TABLE II A list of the specimens heat treated and analysed using a simultaneous DTA/TG thermal analyser

Specimen	Composition	Heating rate (°C h^{-1})	Quench temperature (°C)	Remark
5	123	30	–	Coarse particles
6	123	60	–	Coarse particles
7	123	120	–	Coarse particles
8	123	240	–	Coarse particles
9	123	480	–	Coarse particles
10	90% 123 + 10% 211	120	–	Coarse particles
11	80% 123 + 20% 211	120	–	Coarse particles
12	70% 123 + 30% 211	120	–	Coarse particles
13	60% 123 + 40% 211	120	–	Coarse particles
14	50% 123 + 50% 211	120	–	Coarse particles
15	70% 123 + 30% 211	120	1100	Fine particles
16	70% 123 + 30% 211	120	1023	Fine particles
17	70% 123 + 30% 211	120	1020	Fine particles
18	70% 123 + 30% 211	120	1018	Fine particles
19	70% 123 + 30% 211	120	1015	Fine particles
20	70% 123 + 30% 211	120	1013	Fine particles
21	70% 123 + 30% 211	120	1008	Fine particles

TABLE III Bulk specimens heat treated under different conditions to investigate the effects of expansion and densification during melting

Specimen	Heating rate ($°C h^{-1}$)	Remark
22	30	Green body same as specimen 2
23	20	Green body same as specimen 2
24	10	Green body same as specimen 2
25	10	Green body same as specimen 2; seeded; melt textured

TABLE IV Bulk densities of green bodies prepared using different techniques

Specimen	Preparation technique	Bulk density ($g cm^{-3}$)
1	Die pressing	3.5
2	CIP of specimen 1	4.5
3	Sintering of specimen 1	5.9
4	Sintering of specimen 2	5.3

lower heating rates, as summarized in Table III. Green bodies for these specimens were prepared in exactly the same way as specimen 2 (see Table I). The microstructures of the pellets after melting were studied by optical microscopy of cross-sections prepared by cutting and polishing. A final pellet (specimen 25), prepared from a green body similar to specimen 2, was melt processed using a seeded technique to demonstrate the feasibility of growing large grains of YBCO using the optimized heat-treatment conditions determined by this study. This pellet, with seed, was heated at a rate of $10 °C h^{-1}$ to 1100 °C and then cooled slowly ($2 °C h^{-1}$) through the peritectic temperature to 910 °C to form the 123 phase. A high cooling rate to room temperature was employed to complete the processing of this sample.

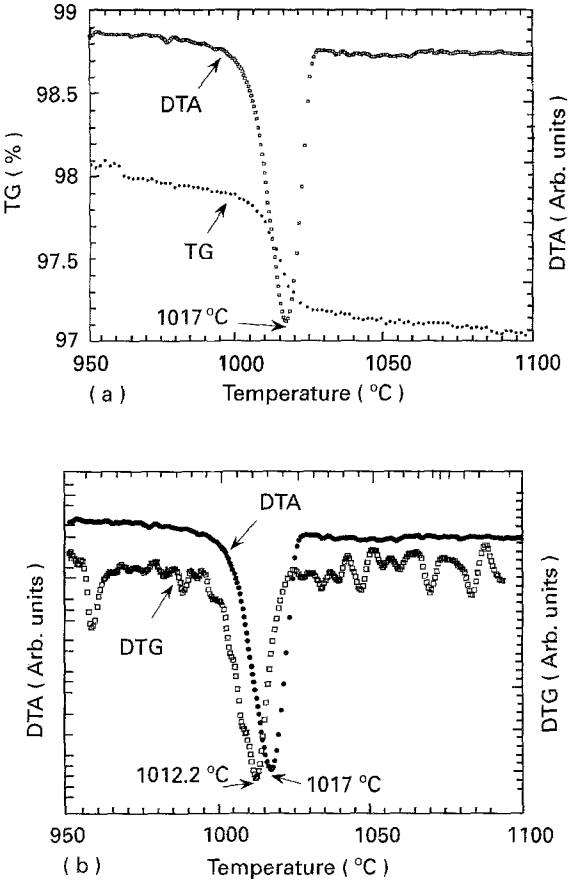

Figure 1 (a) DTA and TG thermographs of specimen 5 which contains only 123 phase material. (b) DTA and DTG thermographs of the same specimen.

3. Results and discussion

3.1. Green body processing

Table IV summarizes the bulk densities of the green bodies resulting from the preparation techniques described in Table I. The pellet after die pressing (specimen 1) exhibits a significantly lower density (~55% theoretical) than that obtained by cold isostatic pressing (~71% theoretical). It may be concluded, therefore, that die pressing alone is not the most appropriate technique for preparing high-density green bodies. Subsequent sintering of both pellets yields a further increase in density (specimens 3 and 4). It can be seen from Table IV, however, that the densification of specimen 3 is greater than that of specimen 4, in contrast to the densities of the as-pressed pellets (specimens 1 and 2). This may be explained by the formation of hard agglomerates during cold isostatic pressing which inhibit grain rearrangement, and consequently limit the efficiency of densification during sintering. It is tempting to conclude from these observations that sintering is the optimum technique for preparing high-density green bodies. However, 211 particles in the bulk of the precursor pellet are likely to coarsen during sintering which is not desirable if a fine distribution of this phase is to be retained and hence this treatment should be avoided if possible. Cold isostatic pressing, therefore, is probably the most practical technique for fabricating green bodies for melt-processing purposes.

3.2. Weight loss during melting

Fig. 1a shows the DTA and TG thermographs of specimen 5, which contains only 123 phase material. The TG thermograph indicates a rapid loss of weight at around 1010 °C corresponding to about 1% of the total specimen weight, which can be attributed to the desorption of oxygen from the 123 phase on heating [15–18]. It can be seen that this process is complete at a temperature close to the peak of the melting endotherm at 1017 °C as determined by the DTA trace (an endotherm signifies absorption of heat by the specimen). The temperature at which the rate of loss of weight by the sample is greatest is about 1012 °C, as indicated by the position of the peak in the DTG thermograph shown in Fig. 1b (i.e. the derivative of the TG curve in Fig. 1a). This is close to the maximum rate of melting of the specimen, which occurs at 1017 °C as shown by the DTA trace. The latter suggests further that melting of this pellet commences at a temperature between 980 and 990 °C.

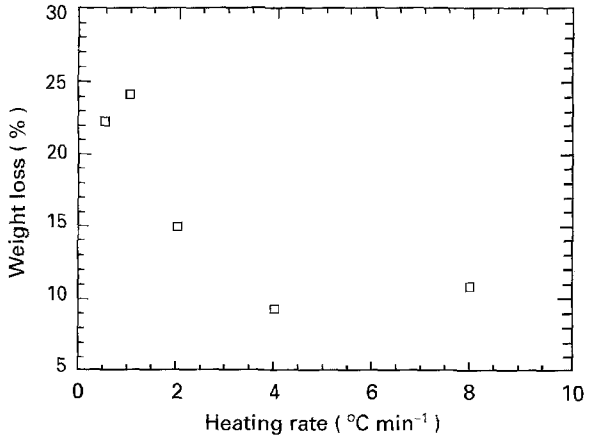

Figure 2 Percentage weight loss of a pure 123 specimen as a function of heating rate.

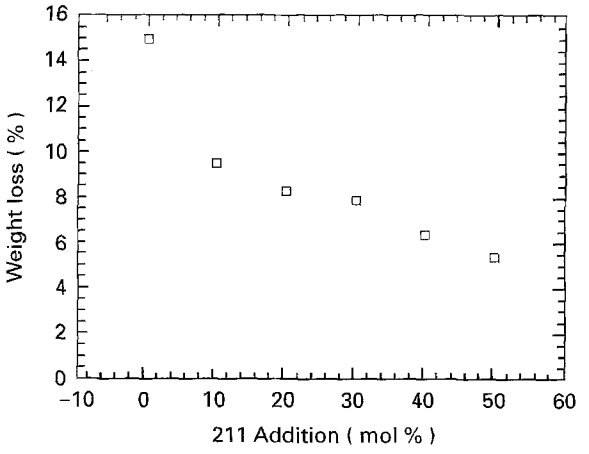

Figure 3 Percentage weight loss as a function of 211 phase content for specimens 7 and 10–14.

The percentage weight loss of the pure 123 phase pellets (specimens 5–9) after rapid cooling from 1100 °C is shown in Fig. 2 as a function of heating rate. This figure shows an obvious dependence of weight loss on heating rate with the greatest loss being observed for heating rates below $\sim 120\,^{\circ}C\,h^{-1}$ ($2\,^{\circ}C\,min^{-1}$). This weight loss is due primarily to loss of liquid from the sample at high temperature. This may be understood by considering the time the sample spends in the incongruently melted state, which effectively doubles as the heating rate is halved. This, therefore, extends the period over which the liquid can migrate from the specimen along the surface of the Al_2O_3 crucible and results in the observed increase in weight loss.

The addition of excess 211 phase to the stoichiometric 123 powder (specimens 10–14) effectively increases the ability of the composite specimen to absorb the liquid phase at high temperature which results in a significant reduction in weight loss at a heating rate of $120\,^{\circ}C\,h^{-1}$, as illustrated by Fig. 3 (this figure also includes data for specimen 7 which was prepared under the same conditions with no 211 enrichment). Specimens 12 and 15, which contained coarse and fine particles, respectively, were processed identically (i.e. heated at the same rate and both cooled rapidly from 1100 °C) in order to investigate the effect of particle

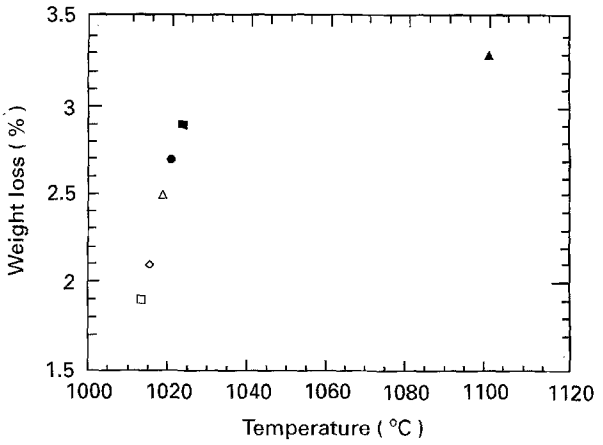

Figure 4 Percentage weight loss during the peritectic melting process of specimens containing submicrometre size 211 phase particles. 30 mol % excess 211 phase was used in each case. Specimen: (○) 21, (□) 20, (◇) 19, (△) 18, (●) 17, (■) 16, (▲) 15.

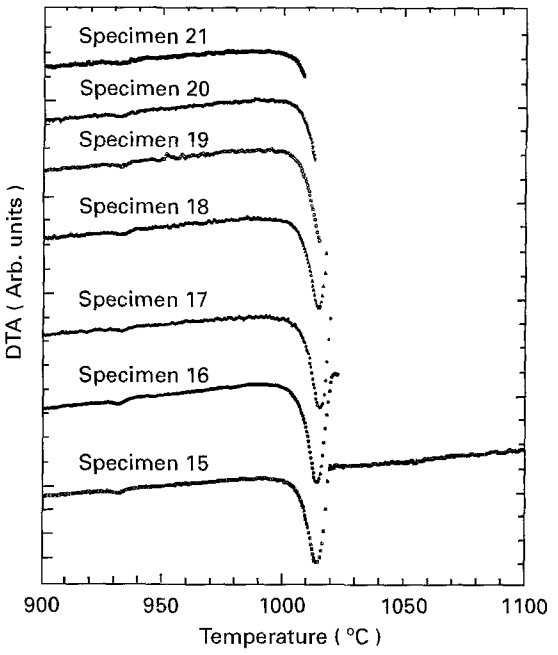

Figure 5 DTA thermographs defining the degree of melting in specimens containing 30 mol % excess submicrometre size 211 phase particles.

size on liquid loss. The total weight loss of the specimen containing coarse particles was found to be about double that containing fine particles due to the lower net surface area of the former, which translates to a reduced ability to absorb liquid in the high-temperature state.

The total percentage weight loss of specimens 15–21 (rapidly cooled from different temperatures) is shown in Fig. 4. This reveals a sharp increase in weight loss between 1010 and 1025 °C, which coincides well with the temperature range of the DTA partial melting endotherm shown in Fig. 1 (this defines the highest rate of partial melting in the specimen). An additional, but less significant, increase in weight loss can be observed in the higher temperature region (up to 1100 °C).

Fig. 5 shows the DTA thermographs of specimens 15–21. These were used to estimate the degree of

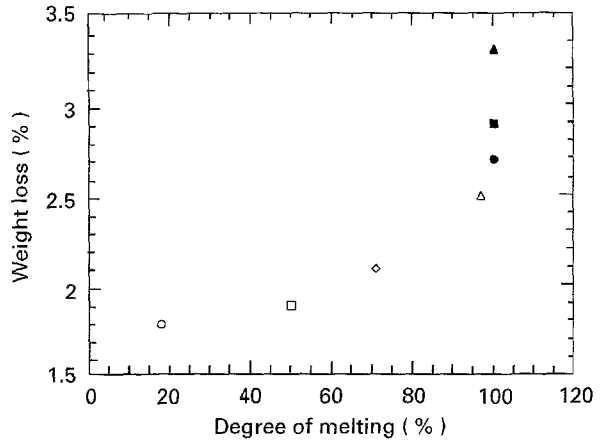

Figure 6 Percentage weight loss as a function of degree of melting for specimens containing 30 mol % excess submicrometre size 211 phase particles. Specimen: (○) 21, (□) 20, (◇) 19, (△) 18, (●) 17, (■) 16, (▲) 15.

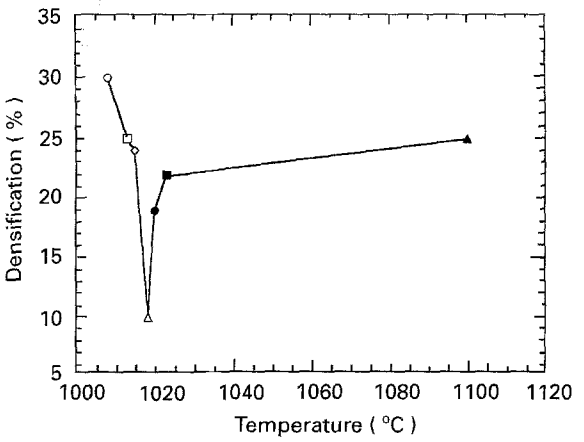

Figure 7 Percentage densification during the peritectic melting process of specimens containing 30 mol % excess submicrometre size 211 phase particles. Specimen: (○) 21, (□) 20, (◇) 19, (△) 18, (●) 17, (■) 16, (▲) 15.

melting of these specimens in an attempt to correlate this variable with percentage weight loss. The DTA endotherms for specimens 15–17 are similar in form to that shown in Fig. 1 which suggests that partial melting in these specimens is complete. This is not the case for specimens 18–21, however, which exhibit incomplete DTA thermographs.

Extrapolation of the baseline through the melting peak in the DTA trace can yield information about the nature of the melting process. A change in baseline, for example, is indicative of a change in the heat capacity of the specimen on melting with the area under the melting peak being proportional to the latent heat of the melting process. The latent heat of melting for specimen 15 may be calculated from its DTA thermograph given that the change in baseline is relatively small. This may then be used to estimate the degree of melting in specimens 18–21, for which the melting process is incomplete. For example, the melting process can be seen to be around 50% complete in specimen 20 because the melting peak is only around 50% defined for this sample. In calculating the areas under the DTA melting peaks, the thermal range of the partial melting process has been assumed to be between temperatures of 990 and 1020 °C. The percentage weight loss of specimens 15–21 is replotted as a function of degree of melting in Fig. 6. It can be seen from this figure that the percentage weight loss is directly proportional to the degree of melting and that the rate of increase of the percentage loss is a maximum when the specimens are almost fully melted (i.e. specimens 17 and 18). This is supported by the results for specimens 15–17 (all fully melted) which indicate that significant weight loss takes place during the phase change to the fully peritectically molten state.

3.3. Expansion and densification during melting

Fig. 7 shows the variation in density increase of specimens 15–21 (cooled rapidly from different temperatures) as a function of temperature from which a sharp drop in this parameter can be seen corresponding to an expansion in sample volume during the initial stages of melting. This effect and the observed subsequent densification of the specimens may be explained by considering two competing processes. Oxygen desorption from the sample increases sharply at the onset of melting as shown by Fig. 1a. Optical microscopy confirms that this results in the formation of pores which corresponds to a relative expansion of the specimen. At higher temperature, however, the surface tension associated with the molten state and the reduced oxygen desorption rate are responsible for densification of the sample. On this basis, therefore, the sharp drop in percentage densification shown in Fig. 7 should correlate with the temperature where the rate of oxygen desorption is a maximum. This is indeed the case, as indicated by the position of the DTG peak shown in Fig. 1b.

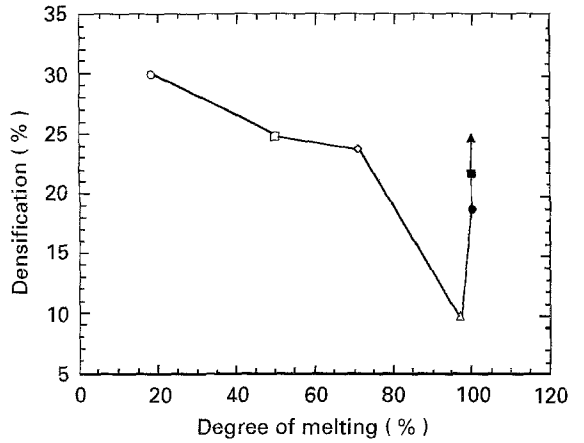

Figure 8 Percentage densification as a function of degree of melting of specimens containing 30 mol % excess submicrometre size 211 phase particles. Specimen: (○) 21, (□) 20, (◇) 19, (△) 18, (●) 17, (■) 16, (▲) 15.

Replotting the percentage densification against degree of melting of the specimens, as presented in Fig. 8, illustrates the expansion of the specimens on melting more clearly. It can be seen that the specimen density decreases gradually as the degree of melting increases until melting is nearly complete (specimen 18). A significant rise in the density is observed, however, as the

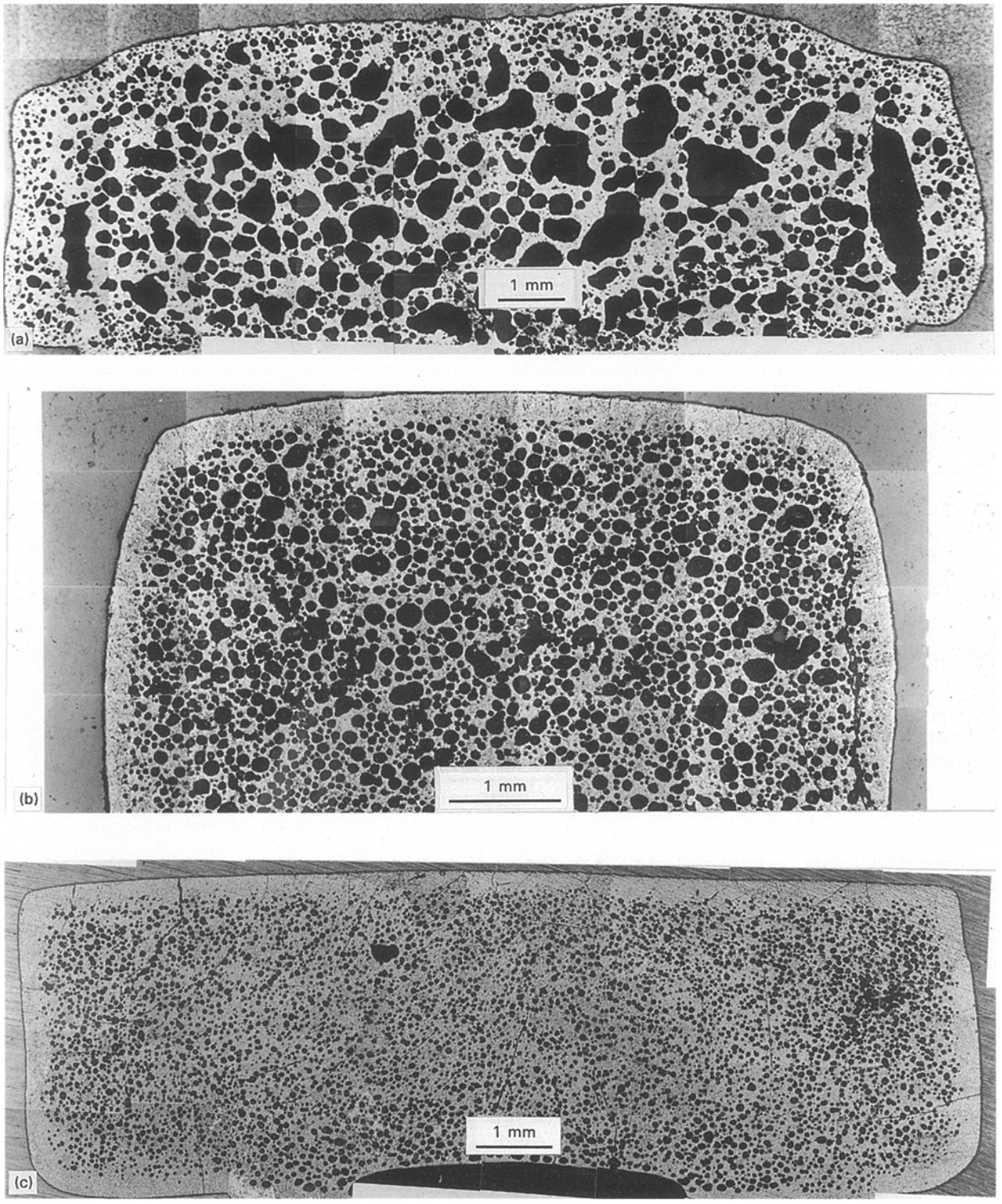

Figure 9 Optical micrographs of polised cross-sections of specimens heat treated at (a) 30 °C h^{-1} (b) 20 °C h^{-1} and (c) 10 °C h^{-1}.

melting process approaches completeness which indicates that surface tension-driven densification is dominant over the effect of oxygen desorption from the sample.

Fig. 9 shows optical micrographs of the polished cross-sections of specimens 22–24 listed in Table III. As summarized in the table, these specimens were heated at rates of 30, 20 and 10 °C h^{-1}, respectively. Although precursor pellets with regular shapes were used for these specimens, the cross-sections presented in Fig. 9 reveal significant differences in the geometry, distribution and structure of the porosity of the pellets after melting. For example, specimen 22 clearly exhibits an expanded region at its centre (Fig. 9a), and contains pores of up to 2 mm diameter throughout its bulk. Specimen 23 also exhibits relatively large pores (typically about 0.2 mm diameter) but with a lower porosity and more uniform geometry (Fig. 9b). A great improvement in the uniformity of the pellet, porosity and pore-size distribution (typically about 50 μm diameter), on the other hand, is observed for specimen 24, which was prepared with the lowest heating rate (Fig. 9c). Reduction of the pore size in this sample by further reduction of the heating rate may not be

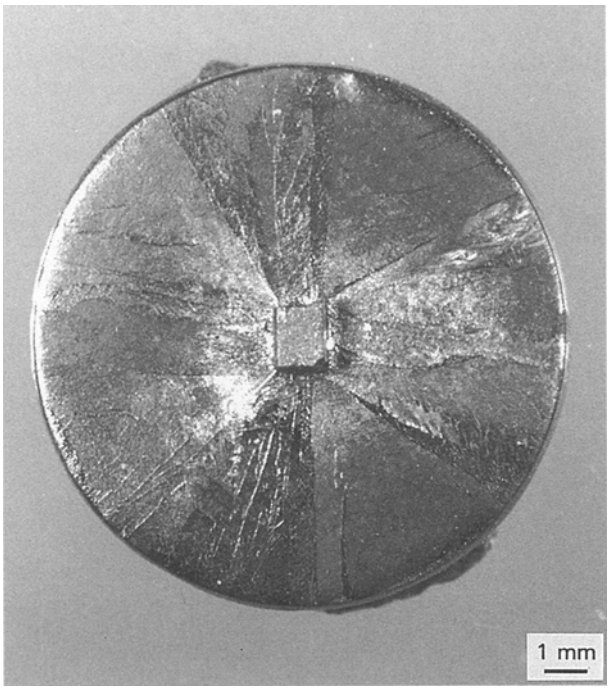

Figure 10 A photograph illustrating the morphology of a seeded melt-textured specimen. The specimen was melted under an optimized heating rate of $10\,°C\,h^{-1}$.

favourable, because this results in an increased loss of liquid from the specimen. This would be extremely undesirable from stoichiometric considerations and would severely limit compositional and grain-size control during melt processing. Further improvements to the physical properties of the specimens, therefore, should be achieved by control of the other processing parameters such as green body density and the peritectic solidification process. Fig. 10 shows a photograph of specimen 25 which was grown using an optimized green body with the properties determined in this study. It can be seen that the sample, which was heated at a rate of $10\,°C\,h^{-1}$ with a single-crystal seed on its surface, is composed of large grains of the 123 phase (i.e. up to 1 cm diameter) and exhibits good homogeneity. This suggests that porosity has been minimized under the thermal processing conditions employed, which was a main objective of the present study.

4. Conclusion

The processing of YBCO ceramics prior to peritectic solidification has been studied in an attempt to identify those properties necessary for the fabrication of large-grain material containing a fine distribution of 211 phase inclusions. The formation of green bodies has been studied with respect to die pressing, cold isostatic pressing and sintering. Although sintering of the die-pressed specimen yielded the highest density, this process produces significant particulate coarsening which inhibits control of the size and distribution of 211 phase inclusions in the melt-processed ceramic. Cold isostatic pressing does not yield the highest green body density but it does preserve the particle size and hence enables better control of the final 211 phase distribution. This method of green body preparation is therefore preferred.

A study of the loss of liquid from the specimens during partial melting and in the partially melted state has revealed that the total percentage weight loss is sensitive to both the heating rate (a lower heating rate gives a higher net percentage weight loss) and proportion of excess 211 phase (percentage weight loss decreases with increased 211 phase content). In addition, the position of the peak of the DTA partial melting endotherm, which defines the position of the greatest rate of melting of the 123 phase, has been observed to correlate with the temperature where the highest rate of liquid loss occurs. It may be concluded from this that the rate of weight loss is maximized when partial melting is almost complete.

Processes responsible for a change in geometry and density of the specimens during partial melting have been identified. The densification process, which tends to eliminate porosity, results from surface tension of the liquid and a capillary effect between the liquid and the 211 phase particles. Expansion of the sample, on the other hand, which takes place close to the onset of partial melting and tends to cause non-uniformity in the specimens, is dominated by the rate of oxygen desorption. The temperature of maximum expansion rate coincides with the maximum rate of oxygen desorption from the sample, which occurs approximately at the position of the DTA partial melting endotherm peak. The expansion process terminates on completion of partial melting whereas the densification process, which is dominated by the volume proportion of liquid, continues but at a reduced rate in the partially molten state. Porosity in the samples cannot be eliminated completely by control of the heating rate alone due to increased liquid loss, and other processing parameters need to be considered if a fully dense material is to be obtained.

Melt processing of large-grain YBCO requires the use of dense green bodies and an optimum heat-treatment process if a fine distribution of 211 phase inclusions and the homogeneity and shape of the sample are to be retained, as demonstrated by the YBCO pellet prepared using a melt-processed seeding technique.

Acknowledgement

One of the authors (W. L.) thanks the Croucher Foundation for financial support in the form of a Research Fellowship.

References

1. M. MURAKAMI, *Supercond. Sci. Technol.* **5** (1992) 185.
2. K. SALAMA, V. SELVAMANICKAM and D. F. LEE, in "Processing and properties of high T_c superconductors, 1: bulk materials", edited by S. Jin (World Scientific, Singapore, 1993) pp. 155–212.
3. M. MORITA, S. TAKEBAYASHI, M. TANAKA, K. KIMURA, K. MIYAMOTO and K. SAWANO, in "Advances in superconductivity III", Proceedings of the 3rd International Symposium Supplement, Sendai, November (1990) pp. 733–6.
4. M. MURAKAMI, M. MORITA, K. DOI and K. MIYAMOTO, *Jpn J. Appl. Phys.* **28** (1989) 1189.

5. A. R. JONES, R. A. DOYLE, F. J. BLUNT and A. M. CAMPBELL, *Phys. C* **196** (1992) 63.
6. A. M. CAMPBELL, D. A. CARDWELL, S. P. ASHWORTH and T. A. COOMBS, "IRC Research Review" (University of Cambridge, UK, 1994) p. 174.
7. H. FUKUYAMA, K. SEKI, T. TAKIZAWA, S. ENDOU, M. MURAKAMI, H. TAKAICHI and N. KOSHIZUKA, *Adv. Supercond.* **5** (1993) 1313.
8. R. TAKAHATA, H. UEYAMA and A. KUBO, *ibid.* **5** (1993) 1309.
9. S. SENGUPTA, D. SHI, Z. WANG, A. C. BIONDO, U. BALACHANDRAN and K. C. GORETTA, *Phys. C* **199** (1992) 43.
10. M. MURAKAMI, S. GOTOH, N. KOSHIZUKA, S. TANAKA, T. MATSUSHITA, S. KAMBE and K. KITAZAWA, *Cryogenics* **30** (1990) 390.
11. K. YAMAGUCHI, M. MURAKAMI, H. FUJIMOTO, S. GOTOH, T. OYAMA, Y. SHIOHARA, N. KOSHIZUKA and S. TANAKA, *J. Mater. Res.* **6** (1991) 1404.
12. Y. YAN, D. A. CARDWELL, A. M. CAMPBELL and W. M. STOBBS, *ibid.* (1994) submitted.
13. M. J. CIMA, M. C. FLEMINGS, A. M. FIGUEREDO, M. NAKADE, H. ISHII, H. D. BRODY and J. S. HAGETY, *J. Appl. Phys.* **72** (1992) 179.
14. W. LO, D. A. CARDWELL, S.-L. DUNG and R. G. BARTER, *J. Mater. Res.* (1994) submitted.
15. W. LO, T. B. TANG, C. LI and Y. XU, *Appl. Phys. Lett.* **53** (1988) 2710.
16. T. B. TANG and W. LO, *Phys. C.* **174** (1991) 463.
17. J. SABRAS, G. PERAUDEAU, R. BERJOAN and C. MONTY, *J. Less-Common Metals* **164–165** (1990) 239.
18. N. H. ANDERSEN, B. LEBECH and H. F. POULSEN, *ibid.* **164–165** (1990) 1172.

Received 27 January
and accepted 22 March 1995